

# Fiber-based polarization-sensitive Mueller matrix optical coherence tomography with continuous source polarization modulation

Shuliang Jiao, Miloš Todorović, George Stoica, and Lihong V. Wang

We report on a new configuration of fiber-based polarization-sensitive Mueller matrix optical coherence tomography that permits the acquisition of the round-trip Jones matrix of a biological sample using only one light source and a single depth scan. In this new configuration, a polarization modulator is used in the source arm to continuously modulate the incident polarization state for both the reference and the sample arms. The Jones matrix of the sample can be calculated from the two frequency terms in the two detection channels. The first term is modulated by the carrier frequency, which is determined by the longitudinal scanning mechanism, whereas the other term is modulated by the beat frequency between the carrier frequency and the second harmonic of the modulation frequency of the polarization modulator. One important feature of this system is that, for the first time to our knowledge, the Jones matrix of the sample can be calculated with a single detection channel and a single measurement when diattenuation is negligible. The system was successfully tested by imaging both standard polarization elements and biological samples. © 2005 Optical Society of America

*OCIS codes:* 120.2130, 170.0170, 170.1870, 170.4500, 260.5430.

## 1. Introduction

Polarization-sensitive (PS) optical coherence tomography (OCT) was first demonstrated in 1992 for measuring tissue birefringence and has been developing quickly since 1997.<sup>1,2</sup> Polarization parameters such as phase retardation and the orientation of birefringence<sup>3–5</sup> were extracted from the measured PS-OCT images by assuming a constant orientation of the birefringence in the sample. Stokes vector images representing the polarization states of the light backreflected from the sample were also constructed.<sup>3</sup> Optical fiber-based PS-OCT was first built in 2000.<sup>6</sup> As a branch of PS-OCT, Mueller matrix OCT merges polarimetry and OCT synergistically, which can provide complete characterization of the polarization properties of a sample by measuring the depth-resolved Jones matrix. To measure a Jones

matrix, usually at least two incident polarization states and two detection channels are needed.<sup>7</sup> The two incident polarization states can be applied either simultaneously by using two independent light sources with different polarization states, like the configuration in our multiple-channel Mueller matrix OCT, or by applying different incident polarization states sequentially by varying the source polarization state with optical polarization elements.<sup>6,8</sup> The multiple-channel Mueller matrix OCT can measure the Jones matrix of a sample with a single measurement.<sup>9,10</sup> The advantage of the sequential implementation is that only one light source is needed. However, the sequential approach requires multiple depth scans (A scans) to calculate the Jones matrix. As a result, a system that can combine the advantages of both of these configurations is highly desirable. To ensure that the information acquired with a single measurement is sufficient for the calculation of the Jones matrix of a sample, one approach is to modulate the source polarization state continuously.

In this paper we report on a new configuration of the fiber-based PS Mueller matrix OCT that permits the acquisition of the round-trip Jones matrix of a biological sample using only one light source and a single depth scan. In this new configuration, a polarization modulator is used in the source arm to continuously modulate the incident polarization state for

---

S. Jiao, M. Todorović, and L. V. Wang (lwang@neo.tamu.edu) are with the Optical Imaging Laboratory, Department of Biomedical Engineering, Texas A&M University, 3120 TAMU, College Station, Texas 77843-3120. G. Stoica is with the Department of Pathobiology, Texas A&M University, College Station, Texas 77843-5547.

Received 27 February 2004; revised manuscript received 14 February 2005; accepted 21 February 2005.

0003-6935/05/265463-05\$15.00/0

© 2005 Optical Society of America

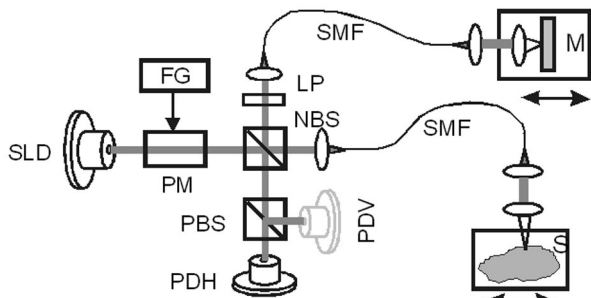


Fig. 1. Schematic of the experimental system. SLD, superluminescent diode, horizontally polarized; PM, polarization modulator; FG, function generator; NBS, nonpolarizing beam splitter; LP, linear polarizer; M, mirror; PBS, polarizing beam splitter; SMF, single-mode optical fiber; PDH and PDV, photodiodes for the horizontal (H) and vertical (V) polarization components, respectively. The vertical channel can be removed when diattenuation can be neglected in a sample (S).

both the reference and the sample arms. The modulation should be fast enough to ensure that several cycles of the incident polarization state can be applied in the scanning range corresponding to the depth resolution of the system.

## 2. Experimental System and the Algorithm for Jones Matrix Calculation

Figure 1 shows a schematic of the experimental system. A superluminescent diode (center wavelength, 850 nm; FWHM bandwidth, 26 nm; output power, 5 mW; horizontally polarized) is used as the low-coherence light source. A polarization modulator (Conoptics), the fast axis of which is oriented at  $45^\circ$ , is used in the source arm to continuously modulate the polarization state of the source beam. A linear polarizer in the reference arm, oriented at  $45^\circ$ , is used to control the polarization state of the reference light. Both the reference and the sample arms are composed of a single-mode optical fiber. A dc motor-driven linear translation stage in the reference arm is used for the depth scan. A depth scan of 1 mm takes 2 s. The combined sample and reference light is split into the horizontal and vertical polarization components by a polarizing beam splitter. The horizontal and vertical polarization components are detected by two photodiodes (PDH and PDV, respectively, in Fig. 1). Upon measuring the interference signals in the two detection channels, the output Jones vector of the sample arm can be determined.

To calculate the Jones matrix of the sample arm, we must know both the incident Jones vector ( $\mathbf{E}_i$ ) and the output Jones vector ( $\mathbf{E}_o$ ) to and from the sample arm.  $\mathbf{E}_i$  is transformed from the Jones vector of the light source ( $[1 \ 0]^T$ , where the superscript  $T$  transposes a row vector into a column vector) by the Jones matrix of the polarization modulator. The Jones matrix of the polarization modulator ( $\mathbf{J}_m$ ) can be expressed as

$$\mathbf{J}_m(\varphi, \pi/4) = \begin{bmatrix} \cos \varphi/2 & i \sin \varphi/2 \\ i \sin \varphi/2 & \cos \varphi/2 \end{bmatrix}, \quad (1)$$

where  $\varphi$  is the phase retardation of the polarization modulator. The incident polarization state for both the sample and the reference arms can be expressed as

$$\mathbf{E}_i = \begin{bmatrix} \cos \varphi/2 \\ i \sin \varphi/2 \end{bmatrix}. \quad (2)$$

The output Jones vector of the sample arm can be expressed as

$$\mathbf{E}_o = \mathbf{J}_T \mathbf{E}_i = \begin{bmatrix} J(1, 1)\cos \varphi/2 + iJ(1, 2)\sin \varphi/2 \\ J(1, 2)\cos \varphi/2 + iJ(2, 2)\sin \varphi/2 \end{bmatrix}, \quad (3)$$

where

$$\mathbf{J}_T = \begin{bmatrix} J(1, 1) & J(1, 2) \\ J(1, 2) & J(2, 2) \end{bmatrix}$$

is the round-trip Jones matrix of the sample arm.  $\mathbf{J}_T$  is transpose symmetric as a result of the Jones reversibility theorem.<sup>11,12</sup> The Jones matrix of the reference arm ( $\mathbf{J}_{\text{ref}}$ ) can be expressed as

$$\mathbf{J}_{\text{ref}} = \mathbf{J}_{lp} \mathbf{J}_{rf2} \mathbf{J}_{lp},$$

$$\mathbf{J}_{lp} = 1/2 \begin{bmatrix} 1 & 1 \\ 1 & 1 \end{bmatrix}, \quad (4)$$

where  $\mathbf{J}_{rf2}$  and  $\mathbf{J}_{lp}$  are the round-trip and one-way Jones matrices of the single-mode optical fiber and the linear polarizer in the reference arm, respectively. The output Jones vector of the reference arm can be expressed as  $\mathbf{E}_{\text{ref}} = \mathbf{J}_{\text{ref}} \mathbf{E}_i$ . We can deduce the following expression:

$$\mathbf{E}_{\text{ref}} = \begin{bmatrix} E_{rh} \\ E_{rv} \end{bmatrix} \exp(i\varphi/2), \quad (5)$$

where  $E_{rh} \exp(i\varphi/2)$  and  $E_{rv} \exp(i\varphi/2)$  are the horizontal and vertical components of the reference electric field.  $E_{rh}$  and  $E_{rv}$  have the same phase and are functions of  $\mathbf{J}_{rf2}$ .

We then have the detected intensities in the horizontal ( $I_x$ ) and vertical ( $I_y$ ) channels:

$$I_x = |E_{rh} \exp[i(\varphi/2 + \bar{k}z_r)] + [J(1, 1)\cos \varphi/2 + iJ(1, 2)\sin \varphi/2] \exp(i\bar{k}z_s)|^2$$

$$= I_{x0} + \tilde{I}_x,$$

$$I_y = |E_{rv} \exp[i(\varphi/2 + \bar{k}z_r)] + [J(1, 2)\cos \varphi/2 + iJ(2, 2)\sin \varphi/2] \exp(i\bar{k}z_s)|^2$$

$$= I_{y0} + \tilde{I}_y, \quad (6)$$

where  $\bar{k}$  is the center wave number of the light source;  $z_s$  and  $z_r$  are the optical path lengths of the sample and reference arms, respectively;  $I_{x0}$  and  $\tilde{I}_x$  are the noninterference and interference parts of the signal in the horizontal channel, respectively; and  $I_{y0}$  and  $\tilde{I}_y$  are the noninterference and interference parts of the signal in the vertical channel, respectively. The interference parts can be further processed as

$$\begin{aligned}\tilde{I}_x &= |E_{rh}| \operatorname{Re}\{[J(1, 1) + J(1, 2)]\exp[-i(\bar{k}z + \varphi_r)] \\ &\quad + [J(1, 1) - J(1, 2)]\exp[-i(\bar{k}z + \varphi + \varphi_r)]\}, \\ \tilde{I}_y &= |E_{rv}| \operatorname{Re}\{[J(1, 2) + J(2, 2)]\exp[-i(\bar{k}z + \varphi_r)] \\ &\quad + [J(1, 2) - J(2, 2)]\exp[-i(\bar{k}z + \varphi + \varphi_r)]\}, \quad (7)\end{aligned}$$

where  $\varphi_r$  is the phase of  $E_{rh}$  and  $E_{rv}$  and  $z$  is the path-length difference between the reference and the sample arms.  $\tilde{I}_x$  and  $\tilde{I}_y$  can be further expanded as

$$\begin{aligned}\tilde{I}_x &= |E_{rx}| |J(1, 1) + J(1, 2)| \cos(\bar{k}z + \varphi_r - \varphi_{x1}) \\ &\quad + |E_{rx}| |J(1, 1) - J(1, 2)| [\cos(\bar{k}z + \varphi_r - \varphi_{x2}) \\ &\quad \times \cos \varphi - \sin(\bar{k}z + \varphi_r - \varphi_{x2})\sin \varphi], \\ \tilde{I}_y &= |E_{ry}| |J(1, 2) + J(2, 2)| \cos(\bar{k}z + \varphi_r - \varphi_{y1}) \\ &\quad + |E_{ry}| |J(1, 2) - J(2, 2)| [\cos(\bar{k}z + \varphi_r - \varphi_{y2}) \\ &\quad \times \cos \varphi - \sin(\bar{k}z + \varphi_r - \varphi_{y2})\sin \varphi], \quad (8)\end{aligned}$$

where  $\varphi_{x1}$ ,  $\varphi_{x2}$ ,  $\varphi_{y1}$ , and  $\varphi_{y2}$  are the phases of  $J(1, 1) + J(1, 2)$ ,  $J(1, 1) - J(1, 2)$ ,  $J(1, 2) + J(2, 2)$ , and  $J(1, 2) - J(2, 2)$ . When the polarization modulator is driven by a sinusoidal wave,  $\varphi = A_0 \sin \omega_m t$ , where  $\omega_m$  is the angular frequency of the driving wave, we have<sup>13</sup>

$$\begin{aligned}\sin \varphi &= \sum_{l=0}^{\infty} 2J_{2l+1}(A_0)\sin[(2l+1)\omega_m t], \\ \cos \varphi &= J_0(A_0) + \sum_{l=1}^{\infty} 2J_{2l}(A_0)\cos[(2l)\omega_m t], \quad (9)\end{aligned}$$

where  $J_0$ ,  $J_{2l+1}$ , and  $J_{2l}$  are the Bessel functions of the first kind of the order of 0,  $2l+1$ , and  $2l$ . When  $A_0 = 2.405$ ,  $J_0(A_0) = 0$ . We then have

$$\begin{aligned}\tilde{I}_x &= |E_{rx}| |J(1, 1) + J(1, 2)| \cos(\bar{k}z + \varphi_r - \varphi_{x1}) \\ &\quad + |E_{rx}| |J(1, 1) - J(1, 2)| \left\{ \cos(\bar{k}z + \varphi_r - \varphi_{x2}) \right. \\ &\quad \times \sum 2J_{2l}(2.405)\cos[(2l)\omega_m t] - \sin(\bar{k}z + \varphi_r - \varphi_{x2}) \\ &\quad \times \sum 2J_{2l+1}(2.405)\sin[(2l+1)\omega_m t] \left. \right\}, \\ \tilde{I}_y &= |E_{ry}| |J(1, 2) + J(2, 2)| \cos(\bar{k}z + \varphi_r - \varphi_{y1}) \\ &\quad + |E_{ry}| |J(1, 2) - J(2, 2)| \left\{ \cos(\bar{k}z + \varphi_r - \varphi_{y2}) \right. \\ &\quad \times \sum 2J_{2l}(2.405)\cos[(2l)\omega_m t] - \sin(\bar{k}z + \varphi_r - \varphi_{y2}) \\ &\quad \times \sum 2J_{2l+1}(2.405)\sin[(2l+1)\omega_m t] \left. \right\}. \quad (10)\end{aligned}$$

The elements of  $\mathbf{J}_T$  can then be calculated as

$$\begin{aligned}J(1, 1) &= 0.5[\tilde{I}_{ax}^*(\bar{k}z) + \tilde{I}_{ax}] \\ &\quad \times (2\omega_m t - \bar{k}z)/J_2(2.405)/|E_{rx}|, \quad (11a)\end{aligned}$$

$$\begin{aligned}J(1, 2) &= 0.5[\tilde{I}_{ax}^*(\bar{k}z) - \tilde{I}_{ax}] \\ &\quad \times (2\omega_m t - \bar{k}z)/J_2(2.405)/|E_{rx}|,\end{aligned}$$

or

$$\begin{aligned}J(1, 2) &= 0.5[\tilde{I}_{ay}^*(\bar{k}z) + \tilde{I}_{ay}] \\ &\quad \times (2\omega_m t - \bar{k}z)/J_2(2.405)/|E_{ry}|, \quad (11b)\end{aligned}$$

$$\begin{aligned}J(2, 2) &= 0.5[\tilde{I}_{ay}^*(\bar{k}z) - \tilde{I}_{ay}] \\ &\quad \times (2\omega_m t - \bar{k}z)/J_2(2.405)/|E_{ry}|, \quad (11c)\end{aligned}$$

where  $\tilde{I}_{ax}$  and  $\tilde{I}_{ay}$  are the analytic signals of  $\tilde{I}_x$  and  $\tilde{I}_y$ , respectively. As a result, the Jones matrix of the sample arm can be calculated with two frequency terms in the horizontal and vertical detection channels. One term is modulated with a frequency that is determined by the depth scan (the carrier frequency), whereas the other term is modulated with the beat frequency between the second harmonic of the modulation frequency of the polarization modulator and the carrier frequency. Other frequency terms can also be used for the calculation.  $J(1, 2)$  can be calculated with the signals in either detection channel. This relationship can be used to balance the two detection channels when the two detectors are not identical.

We note that when diattenuation can be neglected in a sample, we have  $J(2, 2) = J(1, 1)^*$ . In this situation, from Eqs. (11), we can see that  $\mathbf{J}_T$  can be completely calculated from either  $\tilde{I}_x$  or  $\tilde{I}_y$ . As a result, only one detection channel is needed to measure the round-trip Jones matrix for this type of sample.

### 3. Results and Discussion

The polarization modulator was carefully calibrated to ensure that the amplitude of the driving wave  $A_0 = 2.405$ . For the calibration, a mirror was placed between the nonpolarizing beam splitter and the entrance of the sampling fiber. The power spectra of the modulated intensity signals of the reflected light were monitored in both of the two detection channels. According to Eq. (2), the detected modulated intensities ( $I_{cx}$  and  $I_{cy}$ ) can be expressed as

$$\begin{aligned}I_{cx} &\propto 1/2[1 + \cos(\varphi)], \\ I_{cy} &\propto 1/2[1 - \cos(\varphi)], \quad (12)\end{aligned}$$

From Eqs. (9), we can see that there are only the even harmonic terms in  $I_{cx}$  and  $I_{cy}$ . To set the correct working point, the amplitude of the driving wave of

the polarization modulator was adjusted to make

$$\frac{|I_{cx}(2\omega_m)|}{|I_{cx}(4\omega_m)|} = \frac{|I_{cy}(2\omega_m)|}{|I_{cy}(4\omega_m)|} = \frac{J_2(2.405)}{J_4(2.405)}. \quad (13)$$

The system was first tested with a standard polarization element as the sample—a quarter-wave ( $\lambda/4$ ) plate in combination with a mirror. The fast axis of the wave plate was set at various orientations. The polarization modulator was driven by a 1.5 kHz sinusoidal wave. A carrier frequency of 1.2 kHz was generated by the depth scan. The function generator was set at a burst mode and triggered by the data-acquisition board. The data processing included bandpass filtering in the frequency range of 1–2 kHz to pick up the interested frequency terms in the interference signals followed by a Hilbert transformation to build the analytic signals of  $\tilde{I}_x$  and  $\tilde{I}_y$ .  $\mathbf{J}_T$  was then calculated with Eqs. (11). The measured sensitivity of the system is more than 80 dB.

Twenty depth scans were conducted for each orientation of the  $\lambda/4$  plate. The measured Jones matrix of the sampling fiber was used to eliminate its polarization effect.<sup>10</sup> The round-trip retardation and the orientation of the fast axis of the wave plate were calculated from the treated Jones matrix.<sup>12</sup> The calculated mean values and standard deviations for the round-trip retardation and the orientation of the fast axis are shown in Fig. 2. The calculated orientations of the fast axis are in reference to the value when the orientation was set to zero. The calculated round-trip retardation and the orientation of the fast axis match the expected values satisfactorily, which validates the experimental system.

The system was then used to measure biological samples of porcine tendon, rat skin [Berlin Drucrey (BD-IV)], and the septum of a rat heart. The tendon was fixed in a cuvette filled with saline solution and was imaged *ex vivo*, whereas the skin of a rat tail was imaged *in vivo*. The tail was scrubbed with glycerin

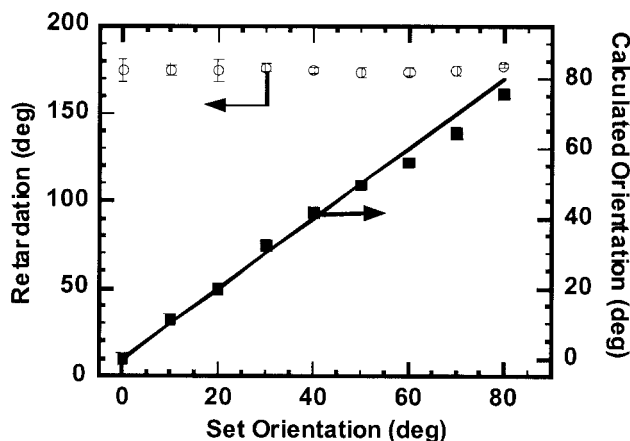


Fig. 2. Mean values and standard deviations of the round-trip retardation and orientation of the fast axis for a  $\lambda/4$  plate calculated from the measured Jones matrix. Most of the error bars are smaller than the size of the marker.

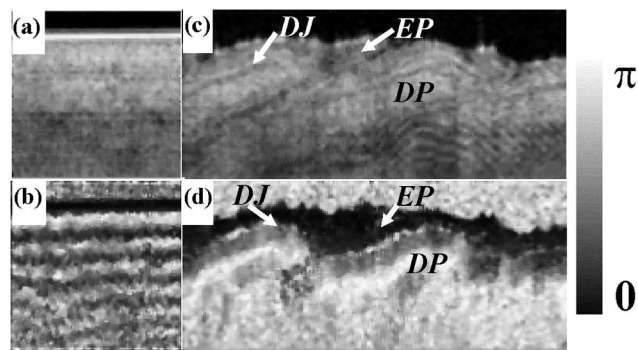


Fig. 3. (a)  $M_{00}$  image of the Mueller matrix and (b) retardation image for a piece of porcine tendon. (c)  $M_{00}$  image of the Mueller matrix and (d) retardation image for the skin of a rat tail measured *in vivo*. The gray scale is for the retardation images. The  $M_{00}$  image is on a logarithmic scale and the retardation images are on a linear scale. The height of each image is 1 mm. EP, epidermis; DP, dermal papilla; DJ, epidermal–dermal junction.

after the hair of the tail was eliminated with hair remover lotion. The samples were translated laterally with a step size of  $10\ \mu\text{m}$  after each A scan. The Jones matrices were calculated and then converted into their corresponding  $4 \times 4$  Mueller matrices.<sup>7</sup> For each sample, the measured Jones matrix at the sample surface was used to eliminate the polarization effect of the sampling fiber.<sup>10</sup> The calculated polarization-independent intensity images (the  $M_{00}$  element of the corresponding Mueller matrix) and the retardation images for the tendon and rat skin samples are shown in Fig. 3. Some structures, like the epidermal–dermal junction and the collagen-rich dermal papillae, can be clearly seen in the images of the rat skin.

The septum of a rat heart was fixed in formalin solution after harvest. The right ventricular side of the septum was imaged. The measured Jones matrix image for a surface layer of  $\sim 40\ \mu\text{m}$  thick was then differentiated with an algorithm developed by our laboratory<sup>14</sup> to yield Jones matrices representing the local polarization properties of the sample. From the differentiated Jones matrices, the orientations of the

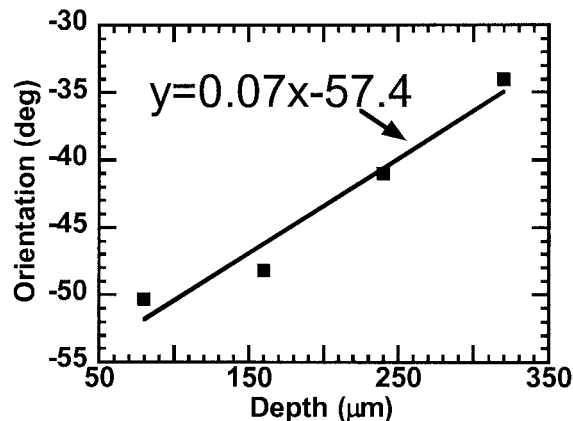


Fig. 4. Muscle fiber orientation in a rat heart septum calculated from the differentiated Jones matrix.

muscle fiber were calculated. As shown in Fig. 4, the calculation revealed that the orientation of the muscle fiber changes with a constant slope of  $\sim 70^\circ/\text{mm}$ , which is in good agreement with histology.<sup>15</sup>

#### 4. Conclusion

In conclusion, we have developed a new model of fiber-based polarization-sensitive Mueller matrix optical coherence tomography that permits the acquisition of the round-trip Jones matrix of a biological sample using only one light source and a single depth scan. A polarization modulator is used in the source arm to continuously modulate the incident polarization states for both the reference and the sample arms. The Jones matrix of the sample can be calculated from the different frequency terms in the two detection channels. For the first time to our knowledge, the Jones matrix of the sample can be calculated with a single detection channel and a single measurement when diattenuation is negligible. The system was successfully applied to image both standard optical elements and biological samples.

This project was sponsored in part by National Institutes of Health grants EB00319-02 and CA092415.

#### References

1. M. R. Hee, D. Huang, E. A. Swanson, and J. G. Fujimoto, "Polarization-sensitive low-coherence reflectometer for birefringence characterization and ranging," *J. Opt. Soc. Am. B* **9**, 903–908 (1992).
2. J. F. de Boer, T. E. Milner, M. J. C. van Gemert, and J. S. Nelson, "Two-dimensional birefringence imaging in biological tissue by polarization-sensitive optical coherence tomography," *Opt. Lett.* **22**, 934–936 (1997).
3. J. F. de Boer, T. E. Milner, and J. S. Nelson, "Determination of the depth-resolved Stokes parameters of light backscattered from turbid media by use of polarization-sensitive optical coherence tomography," *Opt. Lett.* **24**, 300–302 (1999).
4. C. K. Hitzenberger, E. Gotzinger, M. Sticker, M. Pircher, and A. F. Fercher, "Measurement and imaging of birefringence and optic axis orientation by phase resolved polarization sensitive optical coherence tomography," *Opt. Express* **9**, 780–790 (2001).
5. D. P. Davé, T. Akkin, and T. E. Milner, "Polarization-maintaining fiber-based optical low-coherence reflectometer for characterization and ranging of birefringence," *Opt. Lett.* **28**, 1775–1777 (2003).
6. C. E. Saxer, J. F. de Boer, B. H. Park, Y. H. Zhao, Z. P. Chen, and J. S. Nelson, "High-speed fiber-based polarization-sensitive optical coherence tomography of *in vivo* human skin," *Opt. Lett.* **25**, 1355–1357 (2000).
7. S. Jiao and L.-H. V. Wang, "Jones-matrix imaging of biological tissues with quadruple-channel optical coherence tomography," *J. Biomed. Opt.* **7**, 350–358 (2002).
8. J. E. Roth, J. A. Kozak, S. Yazdanfar, A. M. Rollins, and J. A. Izatt, "Simplified method for polarization-sensitive optical coherence tomography," *Opt. Lett.* **26**, 1069–1071 (2001).
9. S. Jiao and L.-H. V. Wang, "Two-dimensional depth-resolved Mueller matrix of biological tissue measured with double-beam polarization-sensitive optical coherence tomography," *Opt. Lett.* **27**, 101–103 (2002).
10. S. Jiao, W. Yu, G. Stoica, and L.-H. V. Wang, "Optical-fiber-based Mueller optical coherence tomography," *Opt. Lett.* **28**, 1206–1208 (2003).
11. N. Vansteenkiste, P. Vignolo, and A. Aspect, "Optical reversibility theorems for polarization: application to remote control of polarization," *J. Opt. Soc. Am. A* **10**, 2240–2245 (1993).
12. S. Jiao, W. Yu, G. Stoica, and L.-H. V. Wang, "Contrast mechanisms in polarization-sensitive Mueller-matrix optical coherence tomography and application in burn imaging," *Appl. Opt.* **42**, 5192–5197 (2003).
13. B. Wang and T. C. Oakberg, "A new instrument for measuring both the magnitude and angle of low level linear birefringence," *Rev. Sci. Instrum.* **70**, 3847–3854 (1999).
14. M. Todorović, S. Jiao, L.-H. V. Wang, and G. Stoica, "Determination of local polarization properties of biological samples in the presence of diattenuation by use of Mueller optical coherence tomography," *Opt. Lett.* **29**, 2402–2404 (2004).
15. P. M. F. Nielsen, I. J. Le Grice, B. H. Smaill, and P. J. Hunter, "Mathematical model of geometry and fibrous structure of the heart," *Am. J. Physiol.* **260**, H1365 (1991).